Journal of Molecular Graphics and Modelling 59 (2015) 123–128

Contents lists available at ScienceDirect

Journal of Molecular Graphics and Modelling

journal homepage: www.elsevier.com/locate/JMGM

Topical perspectives

Structural effects of tachyplesin I and its linear derivative on their aggregation and mobility in lipid bilayers

Eol Han, Hwankyu Lee*

Department of Chemical Engineering, Dankook University, Yongin, 448-701, South Korea

ARTICLE INFO

Article history:
Received 3 February 2015
Received in revised form 9 April 2015
Accepted 17 April 2015
Available online 27 April 2015

Keywords:
Tachyplesin I
Antimicrobial peptide
MD simulation
Lipid bilayer
Peptide–lipid interaction

ABSTRACT

We performed coarse-grained molecular dynamics simulations of tachyplesin I (TP-I), which is a β-hairpin antimicrobial peptide with two disulfide bonds, and its linearly extended derivative without disulfide bonds (TPA4) in lipid bilayers for 5 μs. β-hairpin TP-I peptides tend to individually bind to the bilayer surface, while linear TPA4 peptides aggregate and form the β-strand complex on the bilayer surface, indicating the effect of the peptide structure on aggregation. Also, TPA4 more slowly diffuse along the bilayer surface than do TP-I, indicating that aggregated β-strands of TPA4 cannot diffuse as fast as individual β-hairpins of TP-I. TPA4 have the stronger charge interaction with lipid head groups than do TP-I, leading to the deeper insertion into the bilayer. These simulation results indicate that TP-I peptides tend to individually exist on the bilayer surface and thus easily diffuse along the bilayer surface, while TPA4 peptides aggregate as β-strands, which limits the lateral mobility of TPA4, leading to a strong immobilization of TPA4. These findings agree well with the experimentally observed dependence of peptide mobility on the peptide structure in membranes, as well as support experimental suggestions regarding the formation of β-strand complexes of linear TPA4 and the relationship between the peptide aggregation and mobility.

1. Introduction

Conventional antibiotics such as penicillin and tetramycin have been used to treat microbial infections since their introduction in the mid-1900s, but the problem of resistance to conventional antibiotics has increased [1–3]. To overcome this, development of new antibiotics has been a key issue in modern pharmaceutical industry. Antimicrobial peptides (AMPs), which are short, cationic, and amphiphatic, are among the best candidate antibiotics because they have the potency and specificity to target cell membranes of microbes, leading to cell lysis and death [4]. Tachyplesin I (TP-I), which consists of 17 amino acids with β-hairpin structure, is an AMP extracted from the hemocytes of horseshoe crab [5]. TP-I includes four cysteine (Cys) residues that form two disulfide bridges, leading to a β-hairpin structure. Experiments have shown that TP-I can penetrate into anionic bacterial membranes and induce pore formation, indicating its possible application as novel antibiotics [6,7]. However, TP-I shows high cytotoxicity, which can attack the human cell and thus cause low efficiency of the specific targeting. Also, this β-hairpin peptide with disulfide bonds cannot be easily synthesized, which motivated many experimental studies on the structure and antimicrobial activity for linear derivatives of TP-I.

Matsuzaki et al. pioneered the experimental studies of the structure of TP-I and its derivatives, and their interactions with membranes. They showed that β-hairpin TP-I and linear derivatives induce different extents of membrane disruption and permeability, indicating the dependence on the peptide structure [8,9]. Also, Rao synthesized more various derivatives by replacing four Cys residues with aliphatic hydrophobic, aromatic hydrophobic, and acidic residues, showing that these mutations significantly modulate the secondary structure and antimicrobial activity in membranes [10]. In particular, they found that when Cys residues were replaced with Ala, which is called “TPA4”, its antimicrobial activity significantly decreases, presumably because TPA4 in solution forms a random coil rather than a β-hairpin as observed in experiments by Laederach et al. and Ramamoorthy et al. [11,12]. Polyphemusin I, which is a β-hairpin AMP that consists of amino acids similar to TP-I, was also studied with lipid bilayers by Powers et al., showing that Polyphemusin I promotes lipid flip-flop but does not cause significant vesicle leakage. This implies that the mechanism for the translocation of this peptide may differ from the previously proposed toroidal pore and carpet mechanism [13]. Recently, Doherty et al. showed that both TP-I and its linear

* Corresponding author. Tel.: +82 3180053569.
E-mail address: leeh@dankook.ac.kr (H. Lee).

http://dx.doi.org/10.1016/j.jmgm.2015.04.007
1093-3263/

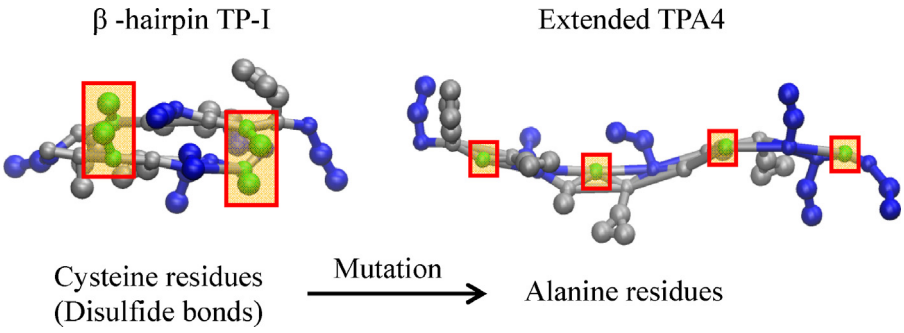

Fig. 1. Structures of the simulated peptides, β-hairpin TP-I and extended TPA4. Gray and blue beads respectively represent hydrophobic and cationic residues, while green beads represent either Cys or Ala residues. The images were generated using visual molecular dynamics [49].

derivatives disorder membranes, but their interactions with membranes differ [14]. Their NMR experiments showed that although both TP-I and TPA4 bind to the bilayer surface, TPA4 is more immobilized on the bilayer than TP-I is, indicating that the peptide structure modulates mobility and activity of peptides [15]. This was explained by suggesting that TP-I peptides diffuse individually along the bilayer surface, while TPA4 may aggregate and form β-strands on the bilayer surface, although the peptide aggregation has not been observed directly from experiments due to the limited resolution.

Molecular dynamics (MD) simulations have been able to explore the structure of AMPs and their interactions with lipid bilayers [16–26]. For β-hairpin TP-I, Boughton et al. simulated TP-I with and without disulfide bonds on the polystyrene surface with explicit water, showing that the predicted interfacial orientation and secondary structure of TP-1 agree well with experimental results [27]. Our group recently simulated polyethylene glycol(PEG)-conjugated TP-I with lipid bilayers, showing that PEGylation influences the binding strength between TP-I and the bilayer surface [28]. However, aggregation and mobility of TP-I and its linear derivatives have not yet been computationally studied.

As a step toward understanding the relationship of secondary structure, aggregation, and mobility of TP-I on membranes, we performed coarse-grained (CG) MD simulations of β-hairpin TP-I and linear TPA4 in phospholipid bilayers. The extent of aggregation is analyzed by calculating the number of peptide clusters and their sizes, which is further verified from calculations of lateral diffusivities of peptides and radial distribution functions between peptides and lipid head groups. We will show that these results support the experimental observations and suggestions regarding the effect of peptide structure on the peptide mobility and interactions with lipid bilayers.

2. Methods

All simulations and analyses were performed using the GROMACS4.5.5 simulation package [29–31]. Models for peptides, palmitoyloleoylglycerophosphoethanolamine (POPE), water, and ions were taken directly from the "MARTINI" lipid and protein force fields (FFs), which lumps a few (three or four) heavy atoms into each CG bead [19,32,33]. POPE lipids were used for bilayers, since experiments have shown that POPE has smaller head group and thus can be more easily disrupted than palmitoyloleoylglycerophosphocholine (POPC), although their mixture with anionic lipids could more realistically reproduce bacterial cell membranes [14,15]. The POPE bilayer (256 POPE/leaflet) was equilibrated in water for 1 μs, showing the area per lipid of 60.1 ± 0.1 Å^2 at 298 K, close to the experimental value of 59 Å^2 at 308 K [34] and the recent simulation result of 59.2 ± 0.3 Å^2 at 310 K [35]. For peptides, TP-I (KWCFR VCYRG ICYRR CR) was modeled as β-hairpin that includes a β-turn around Gly-10, while TPA4 (replacing Cys with Ala; KWAFR VAYRG IAYRR AR) was modeled as the linear (extended) structure (Fig. 1). Note that in the CG model the secondary structure is fixed and thus does not change for the whole simulation time [19]. Here, both β-hairpin and extended structures were also fixed, assuming that these secondary structures do not significantly change in membranes as observed in experiments [14,15]. N- and C-terminal groups were respectively unprotonated and protonated to make them electrostatically neutral, leading to a net charge of +5, which matches the terminal charge state of the experimental peptides [15].

Eight peptides (TP-I or TPA4) were either randomly or regularly positioned above the equilibrated POPE bilayer with a distance of 2.6 nm between the peptide and bilayer centers (Table 1), leading to a peptide:lipid ratio of 1:32, close to experimental ratios of 1:15–1:30 [15]. The final system consists of 16 peptides (8 peptides/leaflet), 512 POPE lipids (256 POPE/leaflet), 12,500 CG water beads (representing ~50,000 real waters), and 96 counterions (Cl^-) in a periodic box of size $12.5 \times 12.5 \times 15$ nm^3. A cutoff of 12 Å was applied for Lennard-Jones (LJ) and Coulomb potentials, which were smoothly shifted to zero between 9 and 12 Å and between 0 and 12 Å, respectively. A temperature of 298 K and a pressure of 1 bar were maintained by applying the velocity-rescale thermostat [36] and Berendsen barostat in the $NP_{xy}P_zT$ ensemble (semi-isotropic pressure coupling) [37]. The LINCS algorithm was used to constrain the bond lengths [38]. To obtain more samples, duplicate simulations were performed for each peptide with each initial configuration (Table 1). Simulations were carried out for 5 μs with a time step of 20 fs at computational facilities supported by the National Institute of Supercomputing and Networking/Korea Institute of Science and Technology Information with supercomputing resources including technical support (KSC-2014-C3-68). The last-3 μs trajectories were averaged for analyses.

3. Results and discussion

3.1. Dependence of peptide aggregation on the peptide structure

TP-I and TPA4 peptides were simulated with lipid bilayers for 5 μs. Fig. 2 shows the initial and final snapshots of peptides in lipid bilayers. Peptides, which were initially regularly or randomly distributed above the bilayer, bind to the bilayer surface but do not insert into the bilayer, as observed in the experiment at such a low concentration of peptides [15]. Regardless of the initial distribution of peptides, linear TPA4 tend to aggregate more significantly than β-hairpin TP-I. To quantitatively analyze this, the number of "clusters" and the number of peptides in the largest cluster were calculated as a function of time, where a "cluster" is either a complex of any size or a free peptide. Here, if the distance between 6th and 13th amino-acid beads of different peptides is less than 0.8 nm,

Table 1
List of simulations.

No. of molecules			Secondary structure	Initial distribution of peptides	No. of simulations
Peptides		POPE			
TP-I	TPA4				
16	–	512	β-Hairpin	Spatially regular	2
16	–	512	β-Hairpin	Spatially random	2
–	16	512	Extended	Spatially regular	2
–	16	512	Extended	Spatially random	2

Table 2
Average numbers of clusters and average numbers of the aggregated peptides in the largest cluster.

	No. of clusters		No. of peptides in the largest cluster	
	Upper layer	Lower layer	Upper layer	Lower layer
TP-I (β-hairpin)	7.2 ± 0.5	7.4 ± 0.3	1.7 ± 0.2	1.6 ± 0.2
	6.8 ± 0.2	6.9 ± 0.2	1.8 ± 0.1	1.9 ± 0.3
	6.4 ± 0.8	7.5 ± 0.2	2.4 ± 0.4	1.4 ± 0.2
	6.6 ± 0.3	6.6 ± 0.2	1.9 ± 0.1	1.9 ± 0.1
TPA4 (extended)	5.8 ± 0.3	5.2 ± 0.6	2.6 ± 0.2	2.7 ± 0.5
	4.2 ± 0.3	6.0 ± 0.4	4.0 ± 0.1	2.1 ± 0.1
	4.9 ± 0.6	6.1 ± 0.4	2.8 ± 0.1	2.4 ± 0.5
	5.5 ± 0.4	5.4 ± 1.0	2.3 ± 0.3	2.8 ± 0.5

then those are considered to be a cluster. Other criteria with the distance from 0.6 to 0.9 nm produce similar qualitative trends. Fig. 3 shows that these both values reach steady states at ~2 μs, indicating the formation of the equilibrated complexes in the bilayer. The number of clusters for TPA4 decreases much more drastically than for TP-I. This is also confirmed from the number of peptides in the largest cluster, showing that the largest cluster consists of 1–2 peptides for TP-I, but ~4 peptides for TPA4. This indicates that TPA4 peptides tend to aggregate and form β-strands on the bilayer surface as visualized in Fig. 3, but TP-I peptides do not. The cluster numbers and sizes for all simulated systems are presented in Table 2, showing the similar tendency of lower cluster numbers and larger cluster sizes for TPA4, although the extents of clustering slightly differ.

This difference in peptide aggregation may be relevant to the peptide conformation. Note that secondary structures of peptides held fixed as explained earlier, and thus TP-I and TPA4 respectively

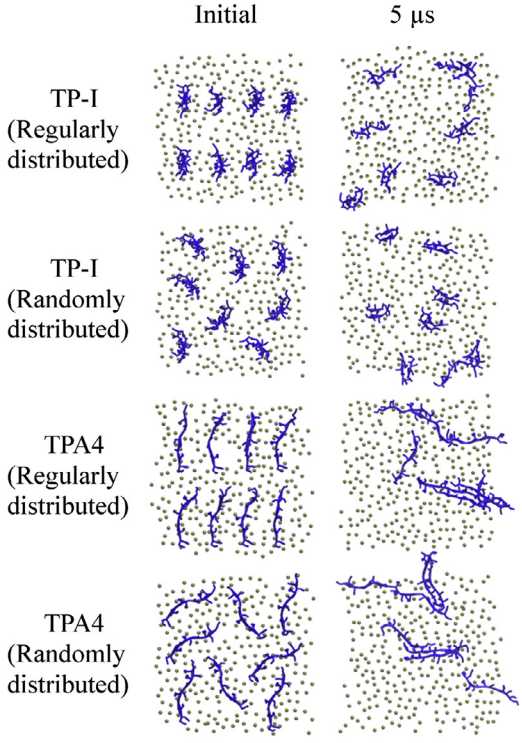

Fig. 2. Snapshots of the top view at the beginning (0 μs; left images) and end (5 μs; right images) of simulations. Lipid phosphates and peptides are represented as brown dots and blue lines, respectively. Note that top views show only one side of the bilayer surface, although peptides are positioned on both leaflets of the bilayer. For clarity, water and ions are omitted.

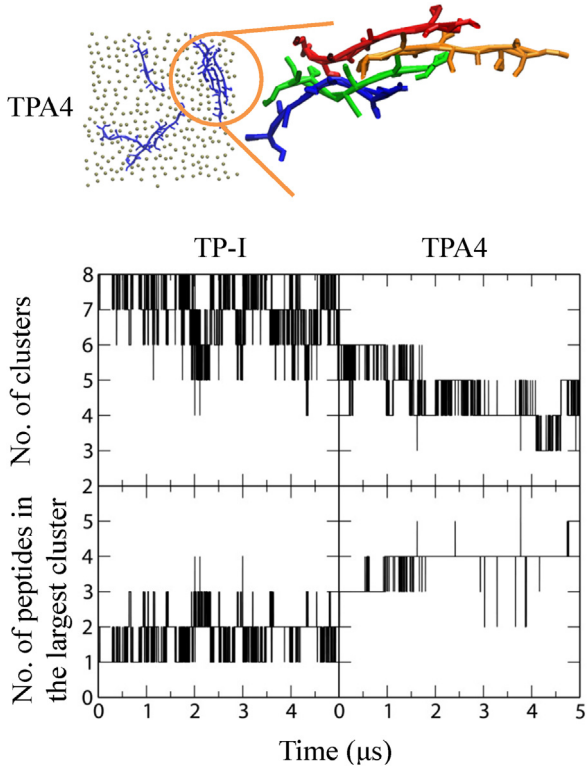

Fig. 3. Number of clusters (top) and number of the aggregated peptides in the largest cluster (bottom) as a function of time. A snapshot at the end (5 μs) of the TPA4 simulation is shown to visualize one of the clusters of TPA4.

Table 3
Average radii of gyration (R_g), aspect ratios, and relative shape anisotropies.

	R_g (nm)	Aspect ratio	Relative shape anisotropy
β-Hairpin TP-I	0.94 ± 0.02	3.02	0.08
Extended TPA4	1.58 ± 0.02	10.54	0.19

retain β-hairpin and extended structures for whole simulation time. These conformations were also quantified by calculating radii of gyration (R_g), aspect ratios, and anisotropies. we computed the aspect ratios, I_z/I_x and I_z/I_y, where I_z, I_y, and I_x are the principal moments of inertia ($I_z > I_y > I_x$) averaged over the last 3 μs of the simulations, and obtained from these the relative shape anisotropy, κ^2 ($\kappa^2 = 1 - 3\ I_2/I_1{}^2$, where I_1 and I_2 are the first and second invariants of the radius of gyration tensor ($I_1 = I_x + I_y + I_z$, $I_2 = I_xI_y + I_yI_z + I_xI_z$)) [39]. A linear array of skeletal atoms is characterized by $\kappa^2 = 1$, while a molecule with tetrahedral or spherical symmetry is characterized by $\kappa^2 = 0$. In Table 3, average radii of gyration for TP-I and TPA4 are respectively 0.94 and 1.58 nm, indicating that TP-I has more compact structure than TPA4, as expected. Also, TP-I and TPA4 respectively show aspect ratios of ~3 and ~11, and relative shape anisotropies of ~0.08 and ~0.19, again confirming that TP-I peptides retain compact structure, while TPA4 is much more linear, apparently because their β-hairpin and extended structure are fixed. These results clearly show that β-hairpin TP-I tend to individually exist on the bilayer, while linear TPA4 aggregate and form clusters, which support the experimental observations that showed that TP-I individually move along the bilayer surface, whereas TPA4 form β-strands.

3.2. The effect of the peptide structure on lateral mobility

Experiments have shown that TPA4 peptides form the cluster as β-strands, and those are relatively more immobilized to the bilayer surface than TP-I peptides are. To investigate this, we calculated lateral diffusion coefficients of peptides, which were calculated from the slopes of the mean-square-displacements (MSDs) of the center of mass (COM) of each peptide in the *xy*-plane (the direction perpendicular to the bilayer normal). Note that for the calculation of MSD from MD simulations of cubic boxes with periodic boundary conditions, the MSD needs to be corrected for finite size effects using Yeh and Hummer's analytic formula [40]. For bilayers in non-cubic boxes, the analytic equation is not clearly formulated yet. Also, the size effect should not significantly influence the comparison of lateral diffusivities because the sizes of simulated systems do not significantly differ. Thus, the finite size effect is not corrected here. With consideration of the rate scaling factor of 4 to account for the speed-up in the diffusion in the CG simulations, Fig. 4 shows that lateral diffusion coefficients of TP-I and TPA4 are respectively 2.9–3.6 × 10^{-8} cm^2/s and 1.1–2.0 × 10^{-8} cm^2/s, indicating that TP-I diffuse along the bilayer surface faster than do TPA4. This is presumably because TP-I individually diffuse along the bilayer surface, while the aggregated TPA4 cannot diffuse as fast as TP-I. These findings support experimental observations of the clustered β-strand structure of TPA4 as well as their lower mobility.

3.3. Interactions between peptides and lipid bilayers

As mentioned above, the aggregated TPA4 laterally diffuse slower than TP-I, showing the higher extent of immobility, which imply that TPA4 more strongly interact with lipid bilayers than do TP-I. To examine this, the distances between COMs of peptides and bilayers in *z*-direction (the bilayer-surface normal) were calculated as a function of time. Fig. 5 shows that the distances between peptides and bilayers are larger for TP-I than for TPA4, indicating

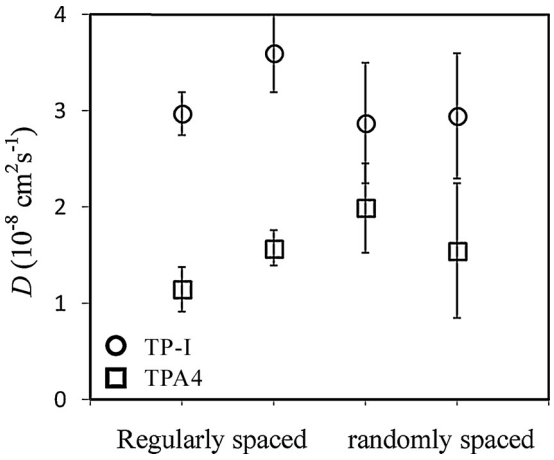

Fig. 4. Lateral diffusion coefficients (D) of peptides in the *xy*-plane (the direction perpendicular to the bilayer normal). The D values for eight simulations are presented, since duplicate simulations were performed for each initial configuration.

that TPA4 more deeply insert into the bilayer than do TP-I. This is also confirmed by calculating radial distribution functions (RDFs) between anionic POPE phosphates and cationic peptide residues. Fig. 6 shows that RDF peaks are higher for TPA4 than for TP-I, regardless of the initial configuration of peptides, which indicates that TPA4 have the stronger charge interaction with the bilayer surface than do TP-I, consistent with the observation of deeper insertion of TPA4 in Fig. 5.

These results, combined with Figs. 3 and 4, indicate that β-hairpin TP-I peptides individually bind to the bilayer surface, while linear TPA4 peptides form the β-strand complexes and more slowly diffuse along the bilayer surface. Also, our simulations show that TPA4 more deeply insert into the bilayer and more strongly interact with lipid headgroups than do TP-I, consistent with the lower mobility of TPA4. These findings agree well with experimental observations of the immobilization of linear TPA4, as well as support the experimental suggestions that the aggregated β-strands of TPA4 cannot diffuse as fast as individual TP-I molecules [15]. These also imply that the oligomerization of those β-strands may significantly influence the antimicrobial activity of TP-I, as also observed in the experiments with α-helical magainin and their derivatives [41–43] and our previous simulations [44]. In this work, our simulations offer insights into the relationship of the peptide structure,

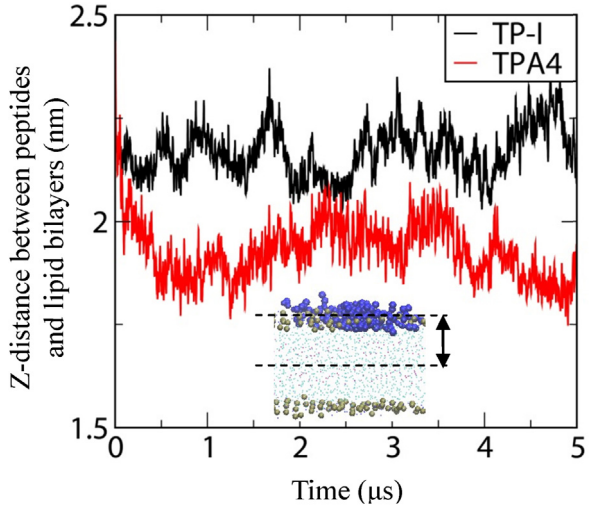

Fig. 5. Average distances between centers of mass of peptides and the bilayer in *z*-direction (the bilayer normal).

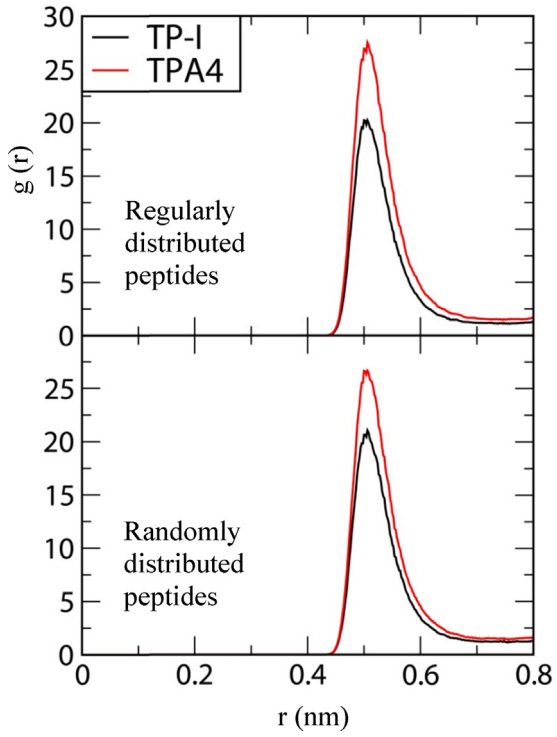

Fig. 6. Radial distribution functions between cationic POPE phosphates and anionic side chains of peptides.

aggregation, and mobility in lipid bilayers, but not antimicrobial activity. In particular, experiments have shown that PE bilayers tend to form negative curvature, which could modulate aggregation and mobility of peptides on the bilayer surface as well as antimicrobial activity [45–48], although bilayer curvature and those effects can be captured only in much larger simulation system. Also, it would obviously be important to understand the key factor controlling the aggregation behavior of linear TPA4, which are worthwhile but beyond the scope of this paper. To understand these, all-atom simulation studies of the peptide aggregation and the interactions between peptides and lipid bilayers ought to be performed at the higher peptide concentration, which we hope to report on elsewhere.

4. Conclusions

Tachyplesin I (TP-I) and its linear derivative (TPA4) were simulated with lipid bilayers using coarse-grained models. TP-I was modeled as a β-hairpin with two disulfide bonds, while TPA4 was generated by replacing four Cys residues of TP-I with Ala residues, leading to linearly extended structure, both of which held fixed for whole simulation time. Starting with random or regular distribution of peptides above the bilayer surface, both TP-I and TPA4 bind to the bilayer surface, but the extents of their aggregation and mobility differ. Most TP-I peptides individually bind to the bilayer surface, showing no peptide aggregation, while TPA4 peptides aggregate and form β-strand clusters on the bilayer surface. This indicates the dependence of peptide aggregation on the peptide structure, as suggested by experiments. Lateral diffusion coefficients of peptides were calculated, showing that TPA4 diffuse slower than TP-I, which indicates that aggregated TPA4 complexes have slower mobility than individual TP-I molecules. Although both TP-I and TPA4 bind to the bilayer surface, TPA4 slightly more deeply insert into the bilayer than do TP-I, showing the charge interaction between peptides and lipid head groups. These simulations successfully capture the experimental observation of the lower mobility of linear TPA4, as well as support experimental suggestions on the structural effect of peptides on their aggregation and mobility in membranes.

Acknowledgment

The present research was conducted by the research fund of Dankook University in 2013.

References

[1] V. Dhople, A. Krukemeyer, A. Ramamoorthy, The human beta-defensin-3, an antibacterial peptide with multiple biological functions, Biochim. Biophys. Acta, Biomembr. 1758 (2006) 1499–1512.
[2] L.M. Gottler, A. Ramamoorthy, Structure, membrane orientation, mechanism, and function of pexiganan—a highly potent antimicrobial peptide designed from magainin, Biochim. Biophys. Acta, Biomembr. 1788 (2009) 1680–1686.
[3] A. Ramamoorthy, Beyond NMR spectra of antimicrobial peptides: dynamical images at atomic resolution and functional insights, Solid State Nucl. Magn. Reson. 35 (2009) 201–207.
[4] M. Zasloff, Antimicrobial peptides of multicellular organisms, Nature 415 (2002) 389–395.
[5] T. Nakamura, H. Furunaka, T. Miyata, F. Tokunaga, T. Muta, S. Iwanaga, et al., Tachyplesin, a class of antimicrobial peptide from the hemocytes of the horseshoe crab (*Tachypleus tridentatus*). Isolation and chemical structure, J. Biol. Chem. 263 (1988) 16709–16713.
[6] J.P. Tam, Y.A. Lu, J.L. Yang, Marked increase in membranolytic selectivity of novel cyclic tachyplesins constrained with an antiparallel two-β strand cystine knot framework, Biochem. Biophys. Res. Commun. 267 (2000) 783–790.
[7] S.A. Muhle, J.P. Tam, Design of gram-negative selective antimicrobial peptides, Biochemistry 40 (2001) 5777–5785.
[8] K. Matsuzaki, S. Yoneyama, N. Fujii, K. Miyajima, K.I. Yamada, Y. Kirino, et al., Membrane permeabilization mechanisms of a cyclic antimicrobial peptide, Tachyplesin I, and its linear analog, Biochemistry 36 (1997) 9799–9806.
[9] K. Matsuzaki, M. Nakayama, M. Fukui, A. Otaka, S. Funakoshi, N. Fujii, et al., Role of disulfide linkages in tachyplesin–lipid interactions, Biochemistry® 32 (1993) 11704–11710.
[10] A.G. Rao, Conformation and antimicrobial activity of linear derivatives of tachyplesin lacking disulfide bonds, Arch. Biochem. Biophys. 361 (1999) 127–134.
[11] A. Laederach, A.H. Andreotti, D.B. Fulton, Solution and micelle-bound structures of tachyplesin I and its active aromatic linear derivatives, Biochemistry 41 (2002) 12359–12368.
[12] A. Ramamoorthy, S. Thennarasu, A. Tan, K. Gottipati, S. Sreekumar, D.L. Heyl, et al., Deletion of all cysteines in tachyplesin I abolishes hemolytic activity and retains antimicrobial activity and lipopolysaccharide selective binding, Biochemistry 45 (2006) 6529–6540.
[13] J.P.S. Powers, A. Tan, A. Ramamoorthy, R.E.W. Hancock, Solution structure and interaction of the antimicrobial polyphemusins with lipid membranes, Biochemistry 44 (2005) 15504–15513.
[14] T. Doherty, A.J. Waring, M. Hong, Peptide–lipid interactions of the β-hairpin antimicrobial peptide tachyplesin and its linear derivatives from solid-state NMR, Biochim. Biophys. Acta, Biomembr. 1758 (2006) 1285–1291.
[15] T. Doherty, A.J. Waring, M. Hong, Dynamic structure of disulfide-removed linear analogs of tachyplesin-I in the lipid bilayer from solid-state NMR, Biochemistry 47 (2008) 1105–1116.
[16] C.M. Shepherd, H.J. Vogel, D.P. Tieleman, Interactions of the designed antimicrobial peptide MB21 and truncated dermaseptin S3 with lipid bilayers: molecular-dynamics simulations, Biochem. J. 370 (2003) 233–243.
[17] A.J. Rzepiela, D. Sengupta, N. Goga, S.J. Marrink, Membrane poration by antimicrobial peptides combining atomistic and coarse-grained descriptions, Faraday Discuss. 144 (2009) 431–443.
[18] D. Peter Tieleman, B. Hess, M.S.P. Sansom, Analysis and evaluation of channel models: simulations of alamethicin, Biophys. J. 83 (2002) 2393–2407.
[19] L. Monticelli, S.K. Kandasamy, X. Periole, R.G. Larson, D.P. Tieleman, S.J. Marrink, The MARTINI coarse-grained force field: extension to proteins, J. Chem. Theory Comput. 4 (2008) 819–834.
[20] E. Mátyus, C. Kandt, D.P. Tieleman, Computer simulation of antimicrobial peptides, Curr. Med. Chem. 14 (2007) 2789–2798.
[21] H. Leontiadou, A.E. Mark, S.J. Marrink, Antimicrobial peptides in action, J. Am. Chem. Soc. 128 (2006) 12156–12161.
[22] P. La Rocca, P.C. Biggin, D.P. Tieleman, M.S.P. Sansom, Simulation studies of the interaction of antimicrobial peptides and lipid bilayers, Biochim. Biophys. Acta, Biomembr. 1462 (1999) 185–200.
[23] S.K. Kandasamy, R.G. Larson, Binding and insertion of α-helical anti-microbial peptides in POPC bilayers studied by molecular dynamics simulations, Chem. Phys. Lipids 132 (2004) 113–132.
[24] P.C. Biggin, M.S.P. Sansom, Interactions of α-helices with lipid bilayers: a review of simulation studies, Biophys. Chem. 76 (1999) 161–183.
[25] W.L. Ash, M.R. Zlomislic, E.O. Oloo, D.P. Tieleman, Computer simulations of membrane proteins, Biochim. Biophys. Acta, Biomembr. 1666 (2004) 158–189.

[26] M.P. Aliste, J.L. MacCallum, D.P. Tieleman, Molecular dynamics simulations of pentapeptides at interfaces: salt bridge and cation-π interactions, Biochemistry 42 (2003) 8976–8987.
[27] A.P. Boughton, K. Nguyen, I. Andricioaei, Z. Chen, Interfacial orientation and secondary structure change in tachyplesin. I: Molecular dynamics and sum frequency generation spectroscopy studies, Langmuir 27 (2011) 14343–14351.
[28] E. Han, H. Lee, Effects of pegylation on the binding interaction of magainin 2 and tachyplesin I with lipid bilayer surface, Langmuir 29 (2013) 14214–14221.
[29] D. Van Der Spoel, E. Lindahl, B. Hess, G. Groenhof, A.E. Mark, H.J.C. Berendsen, GROMACS. Fast, flexible, and free, J. Comput. Chem. 26 (2005) 1701–1718.
[30] E. Lindahl, B. Hess, D. van der Spoel, GROMACS 3.0: a package for molecular simulation and trajectory analysis, J. Mol. Model. 7 (2001) 306–317.
[31] B. Hess, C. Kutzner, D. van der Spoel, E. Lindahl, GROMACS 4: algorithms for highly efficient, load-balanced, and scalable molecular simulation, J. Chem. Theory Comput. 4 (2008) 435–447.
[32] S.J. Marrink, H.J. Risselada, S. Yefimov, D.P. Tieleman, A.H. de Vries, The MARTINI force field: coarse grained model for biomolecular simulations, J. Phys. Chem. B 111 (2007) 7812–7824.
[33] S.J. Marrink, A.H. de Vries, A.E. Mark, Coarse grained model for semiquantitative lipid simulations, J. Phys. Chem. B 108 (2004) 750–760.
[34] M. Rappolt, A. Hickel, F. Bringezu, K. Lohner, Mechanism of the lamellar/inverse hexagonal phase transition examined by high resolution x-ray diffraction, Biophys. J. 84 (2003) 3111–3122.
[35] J.B. Klauda, R.M. Venable, J.A. Freites, J.W. O'Connor, D.J. Tobias, C. Mondragon-Ramirez, et al., Update of the CHARMM all-atom additive force field for lipids: validation on six lipid types, J. Phys. Chem. B 114 (2010) 7830–7843.
[36] G. Bussi, D. Donadio, M. Parrinello, Canonical sampling through velocity rescaling, J. Chem. Phys. 126 (2007) 014101.
[37] H.J.C. Berendsen, J.P.M. Postma, W.F. van Gunsteren, A. DiNola, J.R. Haak, Molecular-dynamics with coupling to an external bath, J. Chem. Phys. 81 (1984) 3684–3690.
[38] B. Hess, P-LINCS. A parallel linear constraint solver for molecular simulation, J. Chem. Theory Comput. 4 (2008) 116–122.
[39] D.N. Theodorou, U.W. Suter, Shape of unperturbed linear-polymers—polypropylene, Macromolecules 18 (1985) 1206–1214.
[40] I.C. Yeh, G. Hummer, System-size dependence of diffusion coefficients and viscosities from molecular dynamics simulations with periodic boundary conditions, J. Phys. Chem. B 108 (2004) 15873–15879.
[41] A. Ramamoorthy, D.K. Lee, J.S. Santos, K.A. Henzler-Wildman, Nitrogen-14 solid-state NMR spectroscopy of aligned phospholipid bilayers to probe peptide–lipid interaction and oligomerization of membrane associated peptides, J. Am. Chem. Soc. 130 (2008) 11023–11029.
[42] A. Ramamoorthy, S. Thennarasu, D.-K. Lee, A. Tan, L. Maloy, Solid-state NMR investigation of the membrane-disrupting mechanism of antimicrobial peptides MSI-78 and MSI-594 derived from magainin 2 and melittin, Biophys. J. 91 (2006) 206–216.
[43] F. Porcelli, B.A. Buck-Koehntop, S. Thennarasu, A. Ramamoorthy, G. Veglia, Structures of the dimeric and monomeric variants of magainin antimicrobial peptides (MSI-78 and MSI-594) in micelles and bilayers, determined by NMR spectroscopy, Biochemistry 45 (2006) 5793–5799.
[44] E. Han, H. Lee, Synergistic effects of magainin 2 and PGLa on their heterodimer formation, aggregation, and insertion into the bilayer, RSC Adv. 5 (2015) 2047–2055.
[45] K.J. Hallock, D.-K. Lee, J. Omnaas, H.I. Mosberg, A. Ramamoorthy, Membrane composition determines Pardaxin's mechanism of lipid bilayer disruption, Biophys. J. 83 (2002) 1004–1013.
[46] K.J. Hallock, D.-K. Lee, A. Ramamoorthy, MSI-78, an analogue of the magainin antimicrobial peptides, disrupts lipid bilayer structure via positive curvature strain, Biophys. J. 84 (2003) 3052–3060.
[47] M.F.M. Sciacca, J.R. Brender, D.K. Lee, A. Ramamoorthy, Phosphatidylethanolamine enhances amyloid fiber-dependent membrane fragmentation, Biochemistry 51 (2012) 7676–7684.
[48] P.E.S. Smith, J.R. Brender, A. Ramamoorthy, Induction of negative curvature as a mechanism of cell toxicity by amyloidogenic peptides: the case of islet amyloid polypeptide, J. Am. Chem. Soc. 131 (2009) 4470–4478.
[49] W. Humphrey, A. Dalke, K.V.M.D. Schulten, Visual molecular dynamics, J. Mol. Graphics 14 (1996) 33–38.